THE JOURNAL OF PHYSICAL CHEMISTRY C

C: Surfaces, Interfaces, Porous Materials, and Catalysis

Distinct Differences in Peptide Adsorption on Palladium and Gold: Introducing a Polarizable Model for Pd(111)

Zak E. Hughes, and Tiffany R. Walsh

J. Phys. Chem. C, **Just Accepted Manuscript** • DOI: 10.1021/acs.jpcc.8b05860 • Publication Date (Web): 07 Aug 2018

Distinct Differences in Peptide Adsorption on Palladium and Gold: Introducing a Polarizable Model for Pd(111)

Zak E. Hughes*,†,‡ and Tiffany R. Walsh*,†

†*Institute for Frontier Materials, Deakin University, Geelong, Vic. 3216, Australia*

‡*Current address: School of Chemistry and Biosciences, University of Bradford, Bradford, BD7 1DP, UK*

E-mail: Z.Hughes@bradford.ac.uk; tiffany.walsh@deakin.edu.au

Abstract

Materials-binding peptides offer promising routes to the production of tailored Pd nanomaterials in aqueous media, enabling the optimization of catalytic properties. However, the atomic-scale details needed to make these advances are relatively scarce and challenging to obtain. Molecular simulations can provide key insights into the structure of peptides adsorbed at the aqueous Pd interface, provided that the force-field can appropriately capture the relevant bio-interface interactions. Here, we introduce and apply a new polarizable force field, PdP-CHARMM, for the simulation of biomolecule–Pd binding under aqueous conditions. PdP-CHARMM was parametrized with density functional theory (DFT) calculations, using a process compatible with similar polarizable force-fields created for Ag and Au surfaces, ultimately enabling a direct comparison of peptide binding modes across these metal substrates. As part of our process for developing PdP-CHARMM, we provide an extensive study of the performance of ten different dispersion-inclusive DFT functionals in recovering biomolecule–Pd(111) binding. We use the functional with best all-round performance to create PdP-CHARMM. We then employ PdP-CHARMM and metadynamics simulations to estimate the adsorption free energy for a range of amino acids at the aqueous Pd(111) interface. Our findings suggest that only His and Met favor direct contact with the Pd substrate, which we attribute to a remarkably robust interfacial solvation layering. Replica-exchange with solute tempering molecular dynamics simulations of two experimentally-identified Pd-binding peptides also indicate surface contact to be chiefly mediated by His and Met residues at aqueous Pd(111). Adsorption of these two peptides was also predicted for the Au(111) interface, revealing distinct differences in both the solvation structure and modes of peptide adsorption at the Au and Pd interfaces. We propose that this sharp contrast in peptide binding is largely due to the differences in interfacial solvent structuring.

Introduction

The use of biomolecules to synthesize, assemble and activate noble metal nanomaterials has transformative potential applicable to a wide range of fields including nanomedicine, bio-sensing and catalysis.[1–3] While recent studies have advanced our understanding of the sequence-dependent structure/function relationships of peptide-based nanomaterials, substantial progress is still required to ensure the systematic exploitation of such materials to realize their full potential.[4,5] In particular, a deeper comprehension of how biomolecules interact with different metallic surfaces is needed, especially if we wish to rationally design bi- or multi-metallic nanomaterials with enhanced catalytic activities.[6–11] While experimental efforts to resolve the molecular-level structure of the biotic/abiotic interface are evolving, at present molecular dynamics (MD) simulations can provide a key complementary approach to elucidate the structure and interactions of biomolecules adsorbed at aqueous metal interfaces.[5,7,12–28] However, the quality of information that can be obtained from molecular simulation is dependent on the model, including the force-field (FF); i.e., how adequately we can capture and describe the interactions between all components of the interface.

The GolP-CHARMM FF is based on the pioneering GolP FF reported by Iori et al.,[29] and describes the interaction of biomolecules with gold surfaces.[16,17] The GolP-CHARMM FF was specifically developed to satisfy three key criteria: to be compatible with the CHARMM family of biomolecule FFs, to capture the effects of polarization at the metal interface via a rigid-rod dipole approach,[29,30] and, to ensure the correct adsorption of species atop metal sites via the use of virtual sites in the outermost surface layer of metal atoms in the metal substrate. Following the same GolP-CHARMM philosophy, an analogous FF for silver interfaces, AgP-CHARMM, was developed,[18] which enabled a systematic comparison (on an equal footing) of peptide adsorption features across the two metal (Au and Ag) surfaces. In this instance we found that, even in the case of gold and silver substrates, these noble metals gave rise to significant differences in peptide adsorption behaviors.[20] Since their development, these two FFs have enabled elucidation of valuable insights into the nature of the peptide-

gold/silver interface, and have enabled the prediction of peptide adsorption free energies that are consistent with available experimental data.[15,23,27] Palladium has valuable catalytic properties, which can be enhanced further by combining it with another metal (often Au) in bi-metallic nanomaterials. Peptides offer a promising route to controlling the growth, composition and topology of such bi-metallic nanomaterials in aqueous media,[6–10] maximizing the catalytic activity. However, to systematically advance new peptide-mediated strategies for the controlled synthesis of Pd-containing nanomaterials, a greater understanding of the similarities and differences in biomolecular adsorption at the Pd and Au/Ag metal interfaces is required. Thus, there is a need for the development of a polarizable bio-interfacial FF for Pd surfaces that is consistent with those already developed for Au and Ag substrates.

One of the major considerations in the development of bio-interface FF parameters is to ensure a reasonable description of the spatial and orientational structuring of liquid water at the interface. The reason for this focus is that these traits are thought to exert a strong influence in directing the adsorption behavior of biomolecules.[23,31,32] For example, there is a strong body of evidence (primarily drawn from molecular simulation sources) that water is more strongly ordered at the (100) surface of noble metals than at the (111) surface, which is reported to confer differences in the adsorption modes of (bio)molecules at the (111) and (100) metal interfaces.[16–19,23,27,33] Density functional theory (DFT) calculations have predicted that, in vacuo, a single molecule of water adsorbs more strongly at the interface of Pd, and Pt, than to Au and Ag.[34–38] This might lead to a more strongly bound, and ordered, first layer of liquid water molecules at the Pd(111) interface compared with the Au/Ag(111) interface,[33,39–41] which is likely to affect how (bio)molecules adsorb to these different aqueous metal interfaces. Therefore, it is important that our FF can provide a physically reasonable description of the Pd(111)-aqueous interface.

Moreover, the structure of the aqueous Pd(111) interface will depend not only on the Pd-water interaction, but also the water-water interaction, meaning that the water model used alongside the biomolecule–metal FF is a key factor in any description of the liquid/solid

interface. Typically the CHARMM FF is used alongside a modified version of the TIP3P water model,[42,43] however, recent studies have suggested that this combination may have scope for refinement, particularly when applied to intrinsically disordered proteins/peptides (IDPs),[44–48] a characteristic that is thought to be shared amongst many metal-binding peptides. One new water model which may be promising in this respect is TIP4P-D. TIP4P-D is a rigid-body water potential that is a re-parametrized version of the original TIP4P model, modified to feature enhanced dispersion interactions. Biomolecule simulations using TIP4P-D have been reported to predict more extended conformations for IDPs.[47,49] Therefore, in this work we also seek to explore how changes to the water model can affect the binding characteristics of peptides adsorbed at the aqueous metal interface. However, we recognize that the CHARMM family of FFs has been specifically developed in harmonization with the modified form of the TIP3P FF. As we will elaborate herein, we understand that any modifications to the pairing of the biomolecule FF and the water FF should be carefully tested[50] prior to use in production simulations. Therefore, the chief aims of this manuscript are to develop a FF for the Pd(111) interface, denoted PdP-CHARMM herein, that is consistent with the already existing GolP-CHARMM and AgP-CHARMM FFs, and then to use PdP-CHARMM to reveal the similarities and differences in peptide adsorption at the aqueous Au(111) and Pd(111) interfaces.

The first step in the development of the FF is to obtain data against which the FF can be parametrized. Due to the dearth of experimental data for the adsorption energies of water (and other relevant small molecules containing different functional groups) to metal surfaces, the GolP-CHARMM and AgP-CHARMM FFs were parametrized from data obtained from in vacuo plane-wave DFT calculations of small organic molecules (containing the functional groups representative of those found in amino-acids, AAs) adsorbed at the metal interfaces. These DFT calculations were performed using the revPBE-vdW-DF functional[51,52] which uses an explicit nonlocal correlation term to approximately capture contributions to the dispersion interaction. The adsorption energies of molecules to the Au(111) and Ag(111)

interfaces obtained using the revPBE-vdW-DF functional were found to be reasonably consistent with reported experimental data.[16,53–57] However, to ensure that the DFT data used to parametrize the PdP-CHARMM FF are reasonable, here we have tested a number of different dispersion-inclusive functionals and compared our findings for each functional against each other and existing experimental data. The PdP-CHARMM FF was then parametrized against the data obtained from the functional that provided the best overall agreement with experimental data. The structure of liquid water at the Au(111) and Pd(111) interfaces was then predicted from MD simulations and compared, using three water models; TIP3P, and two alternative models. Finally, the adsorption features of biomolecules at the aqueous Pd(111) and Au(111) interfaces were investigated; first by predicting the adsorption free energy for a set of representative AAs, and second by predicting and characterizing the adsorption characteristics of two experimentally-identified Pd-binding peptide sequences.

Methods

DFT Calculations

All plane-wave DFT calculations were performed using the Quantum Espresso code, version 5.2.1.[58] All calculations were performed using ultrasoft pseudopotentials with cutoffs for the plane-wave kinetic energy and electron densities of 25 and 200 Ry, respectively. The Gaussian smearing method, with a width of 0.05 Ry, was used for Brillouin zone integration. The SCF calculation convergence threshold was set to 1×10^{-6} Ry for all calculations. For the geometry optimizations a 0.026 eV/Å force convergence criterion was applied; during the single point calculations the forces were checked to ensure the threshold was not exceeded. k-point meshes of $4 \times 4 \times 1$ and $6 \times 8 \times 1$ were used for the geometry optimizations and single point calculations, respectively. These cutoffs (and the convergence criteria) are consistent with those previously used to determine the adsorption energies of a wide range of molecules to the Au(111) and Ag(111) surfaces.[16,18,57]

The Pd(111) interface was constructed from a $p(4 \times 3)$, $p(4 \times 4)$ or $p(6 \times 3)$ supercell, depending on the size of the adsorbate (Table S1 in the Supporting Information). In all cases the palladium slab was four atomic layers thick. All systems had periodic boundary conditions applied in all three dimensions and were constructed such that along the z axis (perpendicular to the slab plane) a distance of at least 10 Å separated the molecule from the periodic image of the slab surface. For the single point energy calculations the cell dimension perpendicular to the surface plane was increased to ensure a distance of at least 15 Å separated the molecule from the periodic image of the slab surface.

The set of 24 adsorbate molecules considered here (Table S1, Supporting Information) was chosen to span the range of functional groups found in the set of naturally occurring AAs, and was consistent with the set of molecules used to generate the GolP-CHARMM and AgP-CHARMM FFs. Initial tests (made with a sub-set of nine adsorbates) compared the results obtained using ten different functionals: revPBE-vdW-DF,[51,52] PBEκ=1-vdW-DF,[59] optB86b-vdW-DF,[60] optB88-vdW-DF,[59] vdW-DF-C09,[61] vdW-DF-cx,[62] vdW-DF2,[63] rev-vdW-DF2,[64] vdW-DF2-C09[61] and rVV10.[65,66] On the basis of these tests, we excluded several functionals due to strong under-binding or over-binding, or due to numerical instability problems. The remainder of the functionals were then used to calculate surface adsorption energies and separation distances for the full set of 24 molecules that were used as AA analogues.

The adsorption energy, E_{ads}, of the adsorbates to the Pd(111) interface was calculated using

$$E_{\mathrm{ads}} = E_{\mathrm{Pd\text{-}mol}} - E_{\mathrm{Pd}} - E_{\mathrm{mol}} \tag{1}$$

where $E_{\mathrm{Pd\text{-}mol}}$ is the energy of the system containing the Pd slab and the adsorbed molecule, E_{Pd} is the energy of the Pd(111) slab alone, and E_{mol} the energy of the molecule alone; each contribution was calculated with the same, consistent periodic cell dimensions. All systems were geometry-optimized with all atoms free to move, prior to the single-point calculations used to determine the final energy. For hydrocarbon and aromatic species, the

separation distance, d_{sep}, of an adsorbate from the Pd(111) interface was defined as the vertical difference in the z-axis value (*i.e.* normal to plane of the surface) between the top layer of metal atoms and the average position of the adsorbates' heavy atoms. For the species containing a heteroatom (excluding phenol, imidazole and indole), the separation distance was defined as the vertical distance between the top layer of metal atoms and the heteroatom.

Fitting the Force-Field

As defined in the GolP-CHARMM[16] and AgP-CHARMM[18] FFs, each substrate metal atom in the PdP-CHARMM FF possesses a rigid-rod dipole, to approximately account for the polarizability of the surface. A full description of the details of the PdP-CHARMM FF is given in the Section 'Development of the PdP-CHARMM force-field' in the Supporting Information. The CHARMM22* FF[67,68] was used to describe the amino acid analogue molecules. To determine how well PdP-CHARMM reproduced the E_{ads} obtained from the DFT calculations, the set of 24 adsorbate molecules were divided into a fitting set and a validation set (as was done previously for GolP-CHARMM and AgP-CHARMM). The parameters for PdP-CHARMM were fitted against the energies and geometries of the molecules in the fitting set, and the FF results for the validation set were then tested against the DFT results. Each set contained species featuring different functional groups: alkanes, aromatics, oxygen-, nitrogen- and sulphur-containing species. In addition, where possible, the types of molecular sites were further distinguished (i.e. hydroxyl oxygen and carbonyl oxygen) and an example of each was placed in each set. Full details of the fitting procedure are given in the Supporting Information. The FF gromacs files are available from the authors upon request.

Molecular Dynamics Simulations

All MD simulations were performed using Gromacs version 5.0[69] with version 2.0 of the PLUMED plugin used for the metadynamics simulations.[70] All simulations were performed in the Canonical (NVT) ensemble, at a temperature of 300 K, controlled using the Nosé-Hoover thermostat,[71,72] with a coupling constant of $\tau = 0.2$ ps. A time step of 1 fs was used throughout, with the Lennard-Jones non-bonded interactions switched off between 10.0 and 11.0 Å, and a cutoff of 11.0 Å used for the particle mesh Ewald (PME) summation.[73]

The simulations at the Pd(111) and Au(111) interfaces were performed using a slab five atomic layers thick and based on a $p(20\times24)$ supercell, giving the cell the lateral dimensions of 56.7×58.9 / 58.6×60.9 Å^2 for Pd/Au. The cell dimension perpendicular to the metal surface was adjusted to a value such that the density of liquid water in the central region between the slabs was consistent with the density of the water model used at room temperature and ambient pressure. As per our implementations of GolP-CHARMM and PdP-CHARMM, the metal atoms in the both the Pd(111) and Au(111) slabs were fixed in space, with the dipoles allowed to freely rotate. The AAs and peptide molecules were described using the CHARMM22* FF,[67,68] together with either the modified TIP3P,[42,43] TIP4P-D[47] or SPC-Fw[74] models used for water. The interactions of the water and adsorbates with the Au(111) surface was described through the use of the GolP-CHARMM FF,[16] while their interaction with the Pd(111) surface was described via the FF derived in the present work.

Simulations of the Aqueous Interface Simulations of the aqueous Pd(111) interface comprised the metal slab and 5562 or 5417 water molecules for the modified-TIP3P/SPC-Fw or TIP4P-D models, respectively. Comparison simulations of the Au(111)-aqueous interface contained 5766 or 5641 water molecules for the modified-TIP3P/SPC-Fw or TIP4P-D models, respectively. For both systems the cell dimension perpendicular to the metal slab was 60 Å. Each system was modeled using standard MD simulation for 10 ns.

Metadynamics Simulations of Amino Acids The adsorption free-energy profiles of six different AAs (Asn, Arg, HisA, Leu, Met and Ser) at the aqueous Pd(111) were determined from multiple walker well-tempered metadynamics simulations.[75–77] The AAs were capped by acetyl and *N*-methyl groups at the N- and C-termini respectively, and modeled according to the protonation state at pH∼7. Histidine was modeled in the unprotonated state only. Each system comprised the amino acid, the Pd(111) slab, 5580 modified TIP3P water molecules, and for Arg, a Cl^- counter-ion. The potential bias in the metadynamics simulations was applied to the position of an atom(s) in the side chain of the AA (Table S2 in the Supporting Information provides further details), along the direction perpendicular to the Pd surface. Four multiple walkers were used for each amino acid. Gaussians of 0.2 Å width were deposited every 1 ps for 125 ns per walker (equivalent to a total simulation time of 500 ns). The initial Gaussian height was set to 0.5 kJ mol^{-1} and a well-tempered metadynamics bias factor of 10 was used. The free energy of adsorption, ΔA_{ads} for each AA was calculated from the integration of the free energy profile as described in the 'Calculation of Free Energy of Adsorption' section of the Supporting Information and following the procedure developed by O'Brien et al.[78]

REST Simulations of Adsorbed Peptides The surface-adsorbed structure(s) of two experimentally identified palladium binding peptides,[1,13] Pd2 (NFMSLPRLGHMH) and Pd4 (TSNAVHPTLRHL), at the aqueous Pd(111) and Au(111) interfaces, were determined using replica exchange with solute tempering (REST) MD simulations.[79,80] The peptide chains were modeled with their termini in the zwitterionic form, corresponding with pH∼7. Likewise all sidechain residues were modeled in a protonation state consistent with a pH∼7, and with all His residues modelled in the unprotonated state. The initial configuration of the peptide in each replica differed, covering a range of different secondary structure motifs, e.g. α-helix, β-turn, PPII helix and random coil. The simulations were performed following the same as outlined in our previous studies.[15,20,81] In brief, for each system the simulation was performed

over sixteen replicas, spanning an 'effective temperature' window of 300-433 K (note that the thermal temperature of each replica was thermostatted to 300 K). The Hamiltonian scaling values, λ, used for the sixteen replicas were 0.000, 0.057, 0.114, 0.177, 0.240, 0.310, 0.382, 0.458, 0.528, 0.597, 0.692, 0.750, 0.803, 0.855, 0.930, 1.000. These values were identified on the basis of previous simulations of peptides at aqueous Au and Ag interfaces.[15,20,81] Each replica was equilibrated at its target Hamiltonian for 0.5 ns, with no exchange moves attempted during this period. For each of the three production REST-MD runs, the system was simulated for 20×10^6 REST-MD steps with exchanges attempted between neighbouring replicas every 1000 time-steps (i.e. every 1 ps). Coordinates were saved every 1000 steps. A residue-surface contact analysis and a peptide backbone cluster analysis were performed for each REST-MD simulation, as described in previous work[15] and re-iterated in the 'Analysis of REST MD simulations' section in the Supporting Information.

Results and Discussion

In Vacuo DFT Calculations

To identify the most appropriate functional for determining the adsorption energies for the full set of adsorbate molecules at the Pd(111) surface, nine different dispersion inclusive functionals were tested against a reference set of molecules, for which experimental adsorption energies are available. By the term "dispersion inclusive", we refer to functionals in which the two-body dispersion contribution is approximately captured in a modified correlation term which is based on charge densities and is seamlessly incorporated into the functional, as opposed to the addition of an empirical dispersion correction term. In addition to considering adsorbates for which experimental binding data exist, we also calculated the adsorption energy of water using all of the functionals in the set. There is no published experimental value for the binding energy of water to the Pd(111) surface, but due to the importance of this interaction, we considered this a necessary requirement. Calculation of adsorption

energies using the optB88-vdW-DF functional were attempted, but it was found that this functional was numerically unstable, as reported in a previous study of adsorbates on the Pt(111) surface.[82] The calculated and reference adsorption energies are summarized in Table 1 and Figure 1, and the separation distances of the adsorbates from the metal surface are given in Table S3, Supporting Information.

Table 1: Adsorption energies ($E_{\mathbf{ads}}$ / kJ mol^{-1}) of molecules at the Pd(111) interface for the test set of molecules, predicted from DFT calculations.

Functional	E_{ads} / kJ mol^{-1}								
	CH_4	C_2H_6	C_3H_8	C_4H_{10}	C_5H_{12}	MeOH	EtOH	C_6H_6	H_2O
Expt. [a]	-16.4[b]	-30.3[b]	-44.5[b]	-56.6[b]	-73.8[b]	-54.8[c]	-54.8[c]	-130.0[d]	-
revPBE-vdW-DF	-18.5	-28.2	-38.0	-48.8	-58.0	-42.2	-49.8	-71.9	-28.6
PBEκ=1-vdW-DF	-22.2	-34.4	-46.4	-58.5	-71.2	-52.6	-63.7	-94.6	-37.1
optB86b-vdW-DF	-22.2	-40.7	-59.2	-76.4	-94.5	-62.2	-76.8	-188.2	-45.5
vdW-DF-cx	-20.4	-38.4	-56.4	-74.1	-91.7	-61.2	-76.0	-210.8	-45.0
vdW-DF-C09	-24.7	-45.8	-67.2	-88.0	-110.2	-69.5	-86.8	-236.1	-47.9
vdW-DF2	-15.9	-26.9	-34.4	-44.8	-53.8	-44.9	-54.0	-72.6	-31.8
rev-vdW-DF2	-16.9	-33.5	-49.2	-64.2	-78.4	-55.3	-67.4	-172.3	-40.9
vdW-DF2-C09	-12.5	-27.3	-43.1	-57.3	-72.3	-51.1	-62.8	-188.1	-38.2
rVV10	-22.7	-42.3	-61.2	-79.2	-97.5	-63.5	-78.6	-146.5	-47.1
PBE+D2						-45.5[c]	-54.3[c]		
PBE+D3	-23.6[b]	-40.8[b]	-55.9[b]	-68.8[b]	-86.9[b]				

[a] Obtained from thermal programmed desorption ; [b] from Ref[83] ; [c] from Ref[84,85] ; [d] from Ref[86]

Table 2 gives the root mean square deviation (RMSD) between the experimental adsorption energies and those predicted by the different functionals. No functional was able to accurately capture the adsorption of all of the molecules in the reference set, with all RMSD values for the full set in excess of 13 kJ mol^{-1}. In comparison, for a test set of molecules at the Au(111) interface, the RMSD between the experimental energies and those calculated using the revPBE-vdW-DF functional was 3.7 kJ mol^{-1}. However, the large RMSD values were in some cases a result of the fact that all functionals (except the rVV10 functional) could not adequately capture the adsorption energy of benzene. In contrast to the other adsorbates that physisorb to the Pd(111) surface, benzene is weakly chemisorbed and as previously reported,[53,55,87] (and similarly for Phenylalanine[88]) the original revPBE-vdW-DF

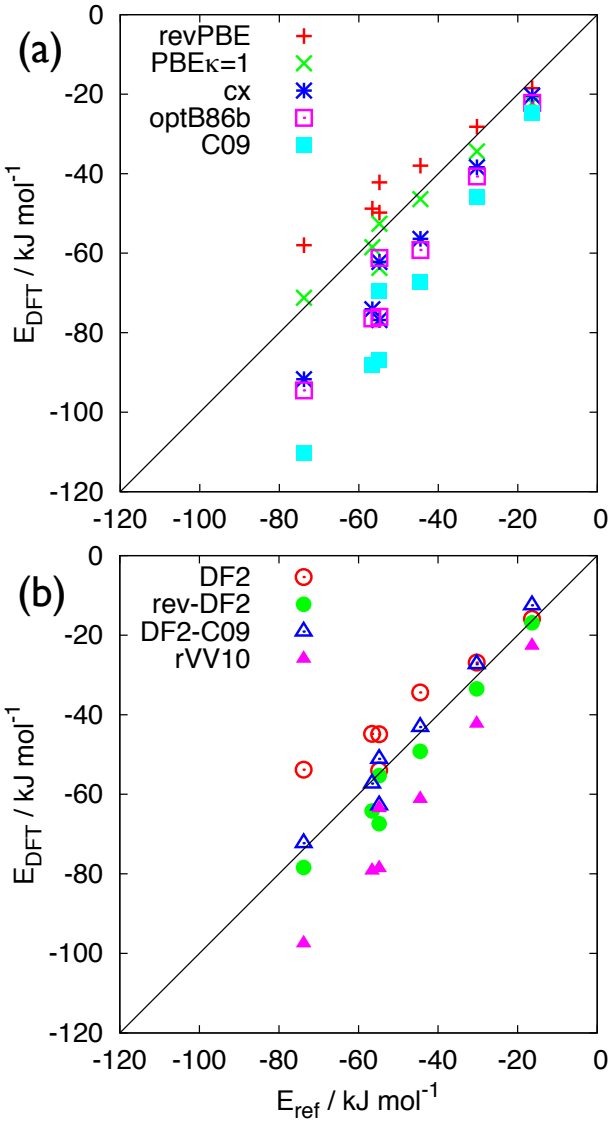

Figure 1: Comparison of binding energies of adsorbate molecules in the test set (excluding benzene) at the Pd(111) surface, predicted by different DFT functionals against the experimental values: (a) for the revPBE-vdW-DF, PBEκ=1-vdW-DF, optB86b-vdW-DF, vdW-DF-cx and vdW-DF-C09 functionals, (b) for the vdW-DF2 rev-vdW-DF2, vdW-DF2-C09 and rVV10 functionals

functional is known to not adequately capture this feature, leading to an under-estimate of the binding energy. This problem is shared by the PBEκ=1-vdW-DF and vdW-DF2 functionals. In contrast, the optB86b-vdW-DF, vdW-CF-cx, vdW-DF-C09, rev-vdW-DF and vdW-DF-C09 functionals appear to overbind benzene on Pd(111). If we exclude benzene from the set, then the RMSD values are significantly improved (except for the rVV10 functional), with the PBEκ=1-vdW-DF, rev-vdW-DF2 and vdW-DF2-C09 functionals performing best. Overall, when compared against experimental data the revPBE-vdW-DF and vdW-DF2 functionals appeared to underbind the adsorbates, while the vdW-CF-cx, optB86b-vdW-DF, vdW-DF-C09 and rVV10 functionals were found to overbind. For comparison, the empirically-corrected PBE+D3 functional yields E_{ads} values for the alkanes that are also too large, with an RMSD across the five molecules of 9.4 kJ mol^{-1}.

Table 2: Root mean squared deviation (RMSD) between the experimental adsorption energies and the corresponding DFT values, using different density functionals.

Functional	RMSD / kJ mol^{-1}		
	Full set	Alkanes	Alkanes and alcohols
revPBE-vdW-DF	22.1	7.2	8.8
PBEκ=1-vdW-DF	13.2	3.0	4.6
optB86b-vdW-DF	25.3	13.0	15.7
vdW-DF-cx	31.4	11.0	13.8
vdW-DF-C09	44.2	21.2	25.0
vdW-DF2	22.5	9.7	10.4
rev-vdW-DF2	16.0	4.0	6.2
vdW-DF2-C09	20.9	2.0	3.9
rVV10	17.5	14.8	17.6

After reviewing our results for the reference set, we decided to calculate the adsorption energies of the full set of molecules using the best performing functionals, namely the PBEκ=1-vdW-DF, rev-vdW-DF2 and vdW-DF2-C09 functionals as well as the revPBE-vdW-DF, optB86b-vdW-DF, and vdW-DF-cx functionals, to determine the binding trends/differences between these functionals. The adsorption energies determined for all 24 adsorbate molecules are summarized in Figure 2, with numerical values provided in Table S4, Supporting Infor-

mation. Figures S1 and S2 show the optimized geometries obtained using the PBEκ=1-vdW-DF functional. Except for the aromatic species (Figure S3), no significant differences in the optimized geometries were observed for the other functionals. In general, the trend in binding strength of E_{ads} followed optB86b-vdW-DF $\approx$ vdW-DF-cx $>$ rev-vdW-DF2 $\geq$ vdW-DF2-C09 $>$ PBEκ=1-vdW-DF $>$ revPBE-vdW-DF. However, the trend across the different molecular species was consistent for all six functionals (Figure 2) with the exception of the aromatic adsorbates, where the chemisorption/physisorption problems discussed above gave rise to significant differences between revPBE-vdW-DF/PBEκ=1-vdW-DF and the other four functionals. There were also some subtle differences between the optB86b-vdW-DF and vdW-DF-cx functionals, with the former more strongly binding the alkanes than the latter, and the reverse behavior for the heteroatomic adsorbates.

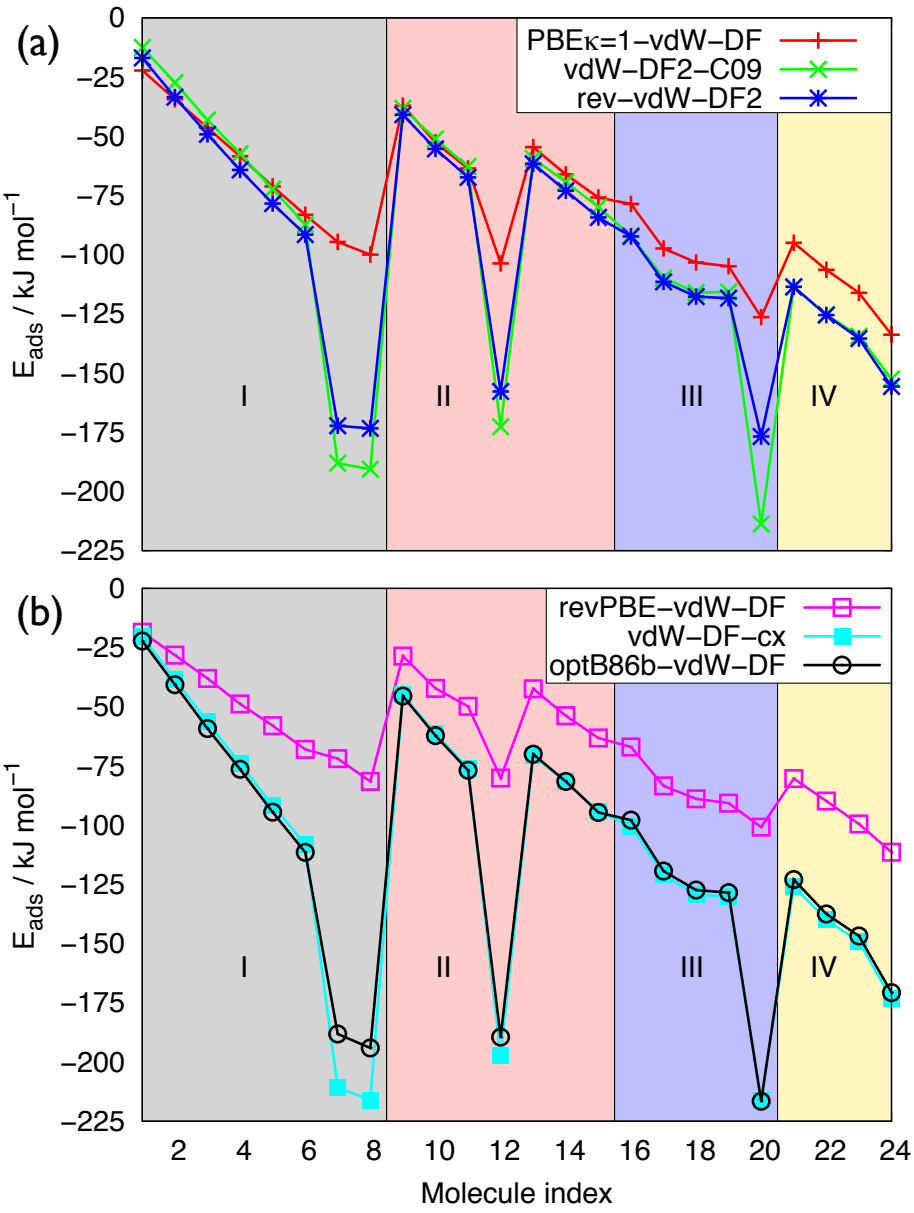

Figure 2: The adsorption energy of molecules to the Pd(111) interface for (a) the PBEκ=1-vdW-DF, rev-vdW-DF2 and vdW-DF2-C09 and (b) the revPBE-vdW-DF, optB86b-vdW-DF and vdW-DF-cx functionals. Lines are a guide to the eye only. Molecule indices are provided in the Supporting Information. Sections I, II, III, and IV correspond to hydrocarbons, oxygen-, nitrogen-, and sulfur-containing adsorbates, respectively.

Comparison of E_{ads} for adsorbates on the Pd(111), Au(111) and Ag(111) surfaces with the revPBD-vdW-DF functional (Table S5), indicated that adsorption was stronger at the Pd(111) interface relative to that at Au/Ag(111), especially for benzene and the heteroatomic species. This trend has been previously observed in the case of water and ethanol,[37,38] but

these results suggest that this could be a common feature for heteroatomic molecules.

Fitting of the Force-Field

Evaluating our DFT results in light of the limited experimental data, the most suitable functionals for fitting the PdP-CHARMM FF appeared to be either the PBEκ=1-vdW-DF and/or the vdW-DF2-C09 functionals. Ultimately we decided to fit to the $E_{\mathrm{ads}}/d_{\mathrm{sep}}$ values of the PBEκ=1-vdW-DF, because, as will be apparent from our results herein, we suspected that phenyl groups may be less likely to chemisorb to Pd(111) under aqueous conditions.

Full details of the parametrization of the PdP-CHARMM FF are given in the Supporting Information section 'Development of the PdP-CHARMM Force-Field'. Briefly, the set of adsorbate molecules was divided into a fitting set and a validation set, with each set containing adsorbates representative of the full range of species. Parameters for the PdP-CHARMM FF were then obtained from fitting against the E_{ads} and d_{sep} values of the molecules in the fitting set, the resulting parameters were then tested against the validation set. Comparisons of the E_{ads} and d_{sep} values obtained via DFT and FF calculations for the fitting and validation sets given in Tables S6 and S7, respectively. The final parameters are summarized in Table 3, alongside corresponding parameters of the AgP-CHARMM and GolP-CHARMM FFs, for convenience of comparison.[16,18]

Pd(111) Aqueous Interface

The structure of liquid water at inorganic solid surfaces is thought to exert a strong influence over how large, complex biomolecules will adsorb to the substrate.[20,23,31–33,89] Therefore, it is a fundamental requirement of our FF to provide a reasonable description of the aqueous Pd(111) interface. The solvation structure of the aqueous Pd(111) interface that was obtained using the modified-TIP3P water model (typically used in conjunction with CHARMM FFs) is shown in Figure 3, with corresponding data for the aqueous Au(111) interface provided for convenience of comparison. As a point of comparison with another

Table 3: Lennard-Jones interaction parameters for the Pd(111) surface. Corresponding parameters for Au(111) and Ag(111) taken from the GolP-CHARM[16] and AgP-CHARMM FFs[18] are shown for comparison (M = metal).

	Pd		Ag[18]		Au[16]	
	σ / Å	ϵ / kJ mol^{-1}	σ / Å	ϵ / kJ mol^{-1}	σ / Å	ϵ / kJ mol^{-1}
M-M	3.65	1.10	3.85	0.41	3.80	0.48
M-M[a] (C sp^2)	2.25	4.00	3.28	0.60	3.20	1.30
M-O (water)	3.00	1.50	3.10	0.90	3.10	0.70
M-O (hydroxyl)	2.90	2.00	3.10	0.90	3.10	0.70
M-O (carbonyl)	2.90	2.00	3.15	0.70	3.10	0.70
M-O (amide)	2.90	2.00	3.10	1.00	3.10	0.70
M-H (water)[b]	2.60	1.00	3.10	0.90	2.70	0.28
M-N (N-Terminal/Lysine)	2.70	6.25	2.85	2.60	2.90	0.90
M-N (imidazole)	2.70	4.25	2.90	1.80	2.85	1.60
M-S	2.75	7.50	2.90	2.40	2.85	3.20

[a] Only applies to the virtual sites not the bulk metal atoms; [b] Also applies to hydroxyl and thiol hydrogens in the case of Ag(111)

metallic interface, solvent structuring at the Ag(111) interface is reported to be similar to that of Au(111), but with a slightly enhanced degree of structuring in the first layer of liquid water molecules.[18] There is encouraging agreement between the classical FF data and findings from first-principles MD (FPMD) simulations in terms of the position of the first peak in the density profile of the water oxygen.[40,41,90] This first peak is located at $\sim$ 2.6 Å from the surface of both metals. The FF simulations indicate that the density of the first layer of water molecules is greater for Pd(111) relative to that of Au(111), which is also consistent with the results of FPMD simulations.[39–41,90–92] We recognize that the relatively shorter time-scales and length-scales of FPMD simulations, as well as the limitations of DFT functionals in describing bulk water,[93] indicate that caution should be used when making quantitative comparisons between FPMD and FF based simulations. Nevertheless, FPMD simulations can provide valuable qualitative information for these interfaces. The enhanced ordering in the first water layer at the Pd(111) interface is also seen in the two-dimensional structuring of the solvent (Figure S4), with water molecules arranged such that they are situated atop metal atoms, again in agreement with FPMD simulations.[39–41,90,91] The hydrogen-bonding network of water molecules at the aqueous Pd(111) interface, while

showing some differences, shares many of the features common to the aqueous Au(111) and Ag(111)[18] interfaces, with a peak in the donor density at the interface (Figures 3(c) and (d)). Additional analyses of the orientational ordering of water molecules at the aqueous Pd(111) and Au(111) interfaces (Figure S5) also reveal similarities between the two metals, with the water molecules closest to the metal interface tilted slightly such that the oxygen is below the hydrogen atoms, denoted as the 'O-down' orientation. However, in agreement with FPMD simulations, we found that the first layer of water molecules at the aqueous Pd(111) interface were more likely to be adsorbed with their dipoles parallel to the interface compared with the Au(111) interface.[40] Additionally, for the successive (i.e. second and third) interfacial solvation layers, the Pd(111) interface appeared to feature greater (i.e. more pronounced) definition in the 'O-down' profile compared with the Au(111) interface. These data provide additional evidence to support the presence of a more structured solvation environment at the Pd(111) interface compared with Au(111).

While the PdP-CHARMM FF produces the correct trend in terms of water being more structured at the Pd(111) than the Au(111)/Ag(111) interfaces, the height of the first peak in the interfacial solvent density profile is greater than might be expected. However, previous simulations reported by Schravendijk *et al.*[94,95] indicated that a very high degree of water structuring is possible for other metal surfaces. In this case these authors reported that the aqueous Ni(111) interface featured a density profile with a first peak ∼50% higher than we have reported here for Pd(111). Nevertheless, we propose this Pd(111) water structuring could conceivably be attributed to the use of the modified TIP3P water model. To investigate the influence of the water model on the aqueous Pd(111) and Au(111) interfaces, we also performed simulations using the TIP4P-D and SPC-Fw water models. The choice of the TIP4P-D model was motivated by recent studies that have indicated the utility of TIP4P-D in describing the extended conformational states of IDPs, compared with traditional water models.[68] Materials-binding peptides that are typically used as capping agents in the synthesis of Pd nanoparticles are often intrinsically disordered. Therefore, it would be

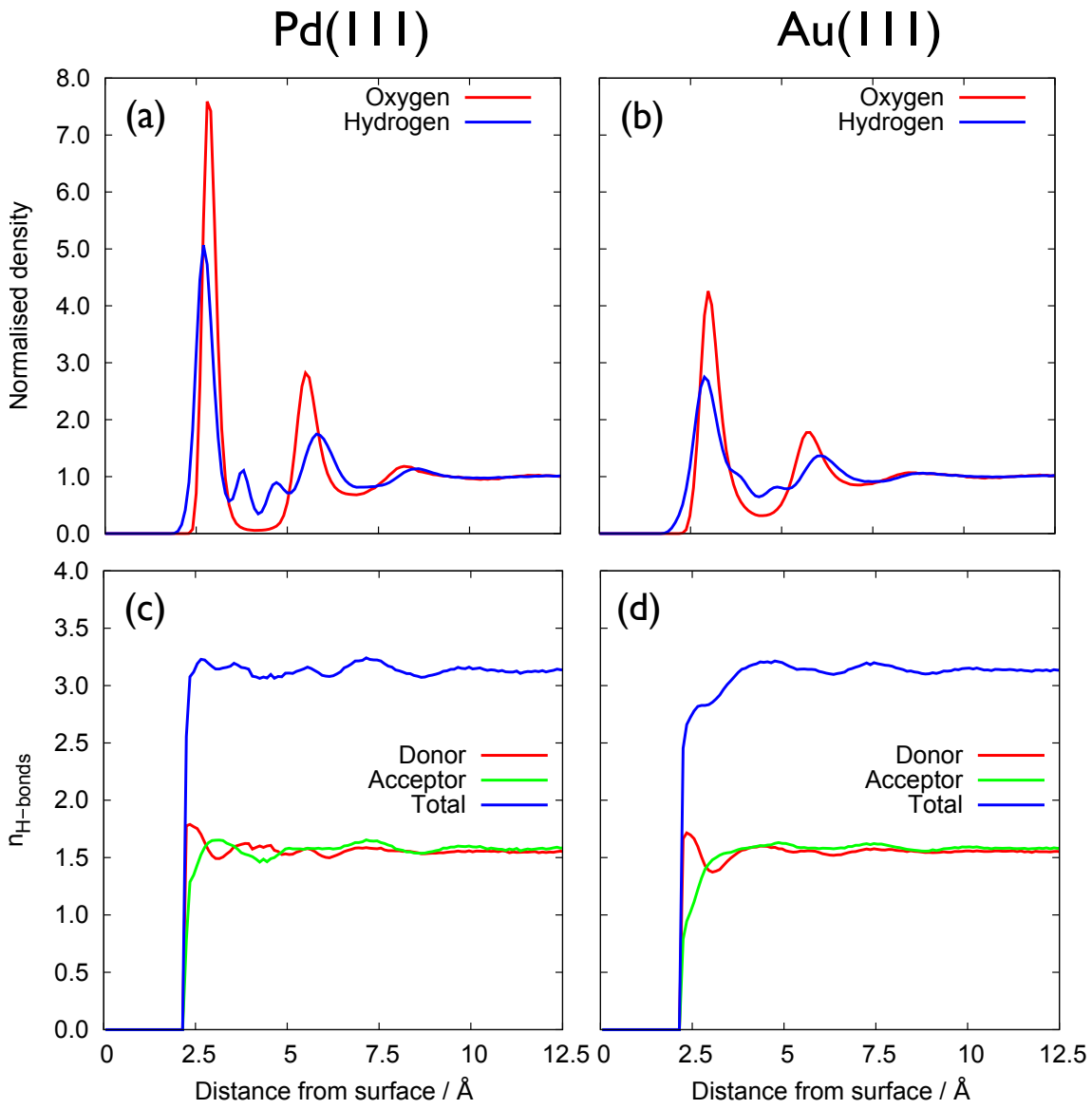

Figure 3: Profiles of water structuring at the aqueous Pd(111) ((a) and (c)) and Au(111) ((b) and (d)) interfaces: (a) and (b) normalized density profiles, (c) and (d) hydrogen-bonding profiles.

informative to model the aqueous Pd(111) interface with the TIP4P-D model. In contrast, the SPC-Fw model is a flexible water model and was chosen as an additional alternative water model. This choice was motivated by simulation data that suggested SPC-Fw to be inter-operable with the CHARMM FFs, providing a similar conformational ensemble to that of the modified TIP3P model for two exemplar tripeptides.[50] We note that the effect of water potential, explored via consideration of the rigid body SPC, SPC/E, TIP3P, TIP4P and TIP5P models, was explored by Schravendijk *et al.*[95] in their study of water structuring at Au(111) and Ni(111) surfaces, and in the adsorption of benzene, phenol, phenylalanine and alanine at the aqueous Ni(111) interface.

We start with calculation of the binding energy of a single water molecule on both the Au(111) and Pd(111) vacuum interfaces using each of the three water models, and compare these with the corresponding DFT data. For all three water models, this adsorption energy of a single water molecule was within 1.3 kJ mol^{-1} of the corresponding DFT value (Table S8), However, bearing in mind that the differences in E_{ads} for the different water models are less than $k_{\text{B}}T$ at room temperature, the trend in binding strength at both interfaces follows TIP4P-D > modified TIP3P > SPC-Fw. We next modeled the structuring of liquid water at the two metal interfaces using all three water models. The density profiles predicted for these different water models (provided in Figure S6) reveal that a high degree of similarity, across both metal surfaces, for the modified TIP3P and SPC-Fw models. This result is consistent with the findings of Schravendijk *et al.*,[95] who compared interfacial solvent structuring of liquid water at the Ni(111) and Au(111) interfaces using different rigid body water models. These authors similarly reported little difference in their density profiles, albeit using a featureless (non-atomistic) description of the metal surface. However, the density profiles for the TIP4P-D model showed some minor differences, notably in the peak heights. Specifically, relative to the other two water models, the height of the first peak in the oxygen profile was somewhat diminished, while that of the second peak was a little amplified in the TIP4P-D profiles. Moreover, the average number of water molecules in the first solvation layer per

surface metal atom was lower (Table S9) for TIP4P-D than that calculated for the interfaces described with the TIP3P and SPC-Fw models. This suggests that for the interface described with the TIP4P-D model, the first solvation layer of water molecules are not bound quite so tightly compared with the interface described with the two other models. The shape of the hydrogen bonding profiles (Figure S7) were similar for all three models, noting that SPC-Fw supported different bulk water behavior to the other two models. However, the orientation profile (Figure S8) of TIP4P-D also differed from that of TIP3P and SPC-Fw, with greater definition in the '2H-down' profile, and less definition in the '1H-down' profile. Minor differences aside, all three of the water models reproduced the same broad trends in water structuring with respect to Pd(111) and Au(111).

Overall, the solvation structure of these aqueous metal interfaces predicted by the GolP-CHARMM, AgP-CHARMM and PdP-CHARMM FFs, and by FPMD simulations, are consistent regarding two key pieces of evidence. First, the the position of the first peak in the interfacial density profile, and second, that the degree of water structuring (strength of layering) follows the trend Pd(111) >> Ag(111) > Au(111). The use of the TIP4P-D or SPC-Fw water models did not radically alter the solvation structure of these aqueous metal interfaces, suggesting that either model may be suitable for use with GolP/AgP/PdP-CHARMM in future studies, subject to other considerations (such as e.g., the balance of the peptide–water interactions).

Biomolecule Adsorption

To further test the PdP-CHARMM FF, we calculated the adsorption free energy at the aqueous Pd(111) interface for six exemplar AAs; Asn, Arg, Leu, Met, His and Ser. These specific AAs were chosen because they are common to both the Pd2 (NFMSLPRLGHMH) and Pd4 (TSNAVHPTLRHL) peptide sequences that have been experimentally identified as Pd binders.[1,13] Moreover, these AAs also cover a range of different side-chain chemistries. We used metadynamics simulations to determine the change in free energy as a function of

distance from the aqueous Pd(111) interface. Evidence of equilibration of the metadynamics simulations is provided in Figure S9.

The effect of the strongly-bound first solvation layer in liquid water is evident from the free-energy profiles for the AAs at the Pd(111) interface (Figure 4). Notably, only His and Met supported a free energy minimum corresponding with a directly bound interfacial state. The remaining AAs typically adsorbed in a solvent-separated interfacial state, where the adsorbate was located at a vertical distance from the surface that approximately corresponded with the second solvation layer. This can be seen from representative configurations of each of the AAs at the position of the global free-energy minimum in each of their respective free energy profiles, provided in Figure 5. Even for those AAs that supported a stable directly-adsorbed binding state, namely Met and His, a substantial energy barrier (with a barrier height $>>$ than k_BT at room temperature) was predicted to lie between the directly-bound state and the solvated-separated state. Moreover, for both His and Met, the well-depths of the directly-bound and solvent-separated states were both very similar and relatively shallow. This combination of a high barrier with similarly-shallow minima confers a rugged free energy landscape regarding interfacial adsorption. This rugged landscape indicates that persistent direct-contact binding for Met and His could be attributed to kinetic trapping (i.e. metastable binding), and cannot be explained by thermodynamic factors, Table 4. The barrier to escape the shallow direct-contact state is $>>$ k_BT at room temperature for both Met and His. These findings are not without precedent. Due to the presence of the remarkably strong interfacial solvent structuring predicted by Schravendijk *et al.*[94,95] for the aqueous Ni(111) interface, these authors also reported that benzene and phenol faced barriers of $\sim$60 and $\sim$24 kJ mol^{-1} to adsorption/desorption at the surface. We note that the solvent structuring predicted for Ni(111) was around 50% greater than what we have predicted for Pd(111). The differing character of our adsorbates (compared with Schravendijk *et al.*) notwithstanding, our predicted barriers to adsorption/desorption are certainly consistent with this earlier result.

The remaining AAs supported free energy profiles with shallow, distant minima, without the presence of substantial intervening energy barriers. These free energy profiles differed markedly from those calculated for the adsorption of AAs at the Au(111) and Ag(111) interfaces, where all AA species have a minimum at a distance of ~ 2.5 Å, from the surface.[20] The current Pd(111) data (particularly the Ser profile) share some similarities with those obtained for AA adsorption at the aqueous Au(100) interface, which also features a strongly bound first layer of water molecules.[27]

We also examined the influence of the water model on AA adsorption. The adsorption free energies of HisA and Ser at the Pd(111) interface were also calculated for the TIP4P-D water model, with no significant differences from the values predicted for the modified TIP3P water model. The free energy profiles were found to be similar across the two water models (Figure S10), although the more extended water layering of TIP4P-D gave rise to a larger peak at ~ 7.5 Å. Schravendijk *et al.* similarly found that the choice of rigid body water model did not significantly modify the (large) barriers to adsorption/desorption for benzene and phenol at the aqueous Ni(111) interface, although these models lacked an atomistic-level description of the metal surface.

Table 4: Free energy of adsorption ($\Delta A_{\mathbf{ads}}$/kJ mol^{-1}) for amino acids at the Pd(111) interface.

Amino acid	ΔA_{ads} / kJ mol^{-1}		
	Pd(111) TIP3P	Pd(111) TIP4P-D	Au(111) TIP3P
Arg	0.0 ± 0.5		
Asn	0.4 ± 0.4		
HisA	-0.3 ± 0.7	-0.4 ± 0.6	-10.7 ± 0.8^a
Leu	0.8 ± 0.3		
Met	-4.0 ± 1.9		
Ser	0.2 ± 0.4	0.6 ± 0.3	-2.5 ± 1.0^a

[a] Adapted from Ref[27]

After considering the adsorption behavior of individual AAs, we then performed REST MD simulations to determine the conformational ensemble of both the Pd2 and Pd4 peptides adsorbed at the aqueous Pd(111) interface. We accomplished this using both the modified

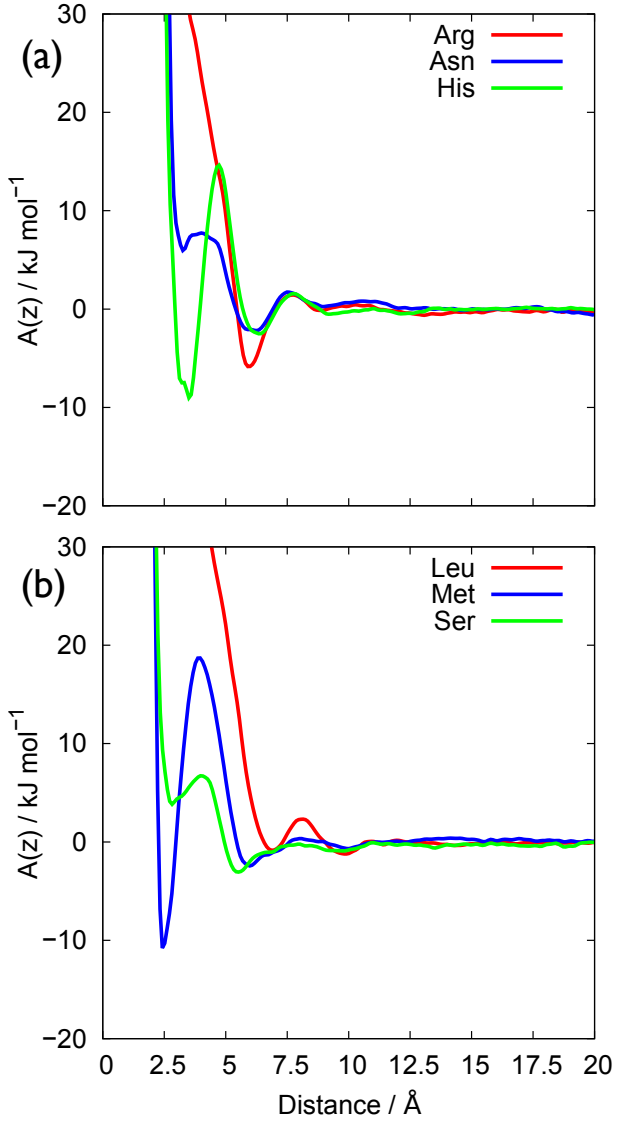

Figure 4: Profiles of the adsorption free energy calculated for (a) Arg, Asn and HisA and (b) Leu, Met and Ser at the aqueous Pd(111) interface.

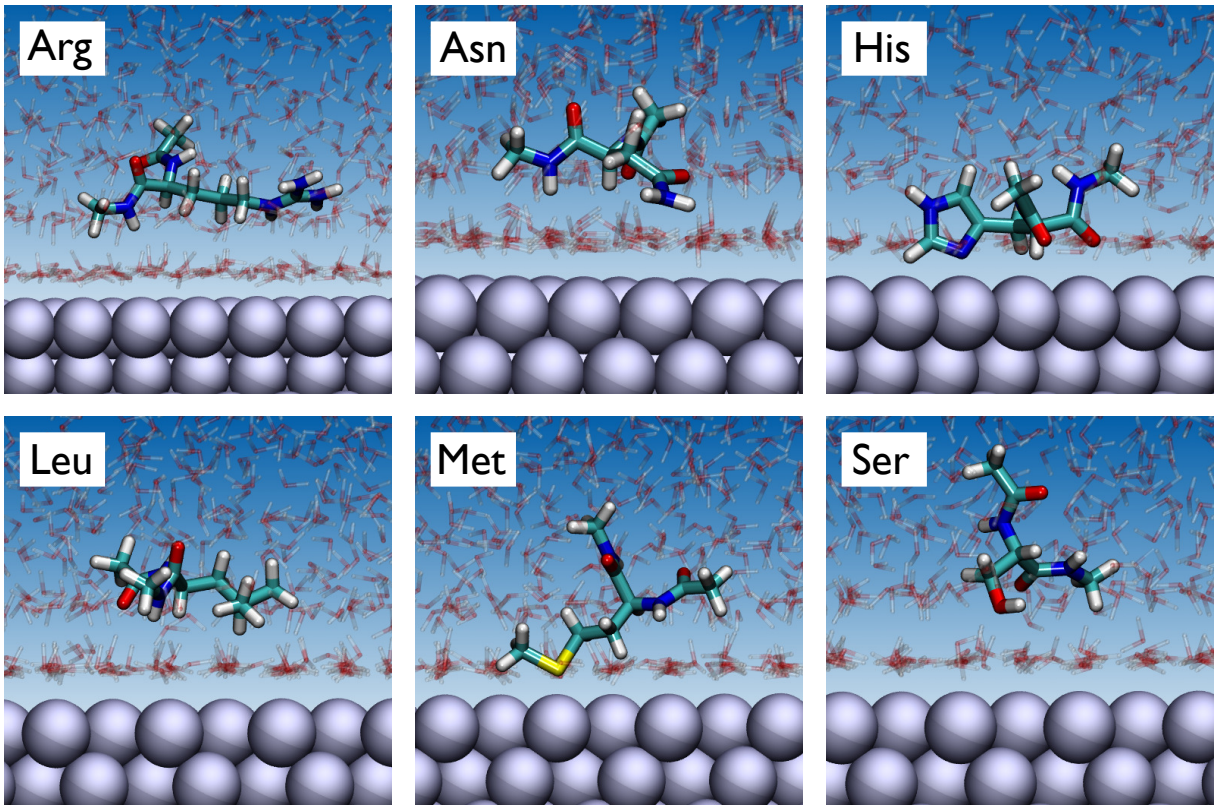

Figure 5: Representative snapshots of the conformations of the AAs at the position of the global minimum in the free energy profile when adsorbed at the aqueous Pd(111) interface.

TIP3P and TIP4P-D water models. While the choice of water model was shown to not appreciably modify the interfacial water structuring or the binding free energies of amino acids at Pd(111), the choice of water model may exert a more profound influence on the conformational ensemble of a peptide when adsorbed at the Pd(111) interface. Furthermore, we also performed REST MD simulations of Pd2 and Pd4 adsorbed at the Au(111) interface.

Representative snapshots of the adsorbed peptides at the two interfaces are provided in Figures 6 and S11. In addition, analysis of the degree of residue-surface contact (in this instance, direct contact with the metal surface) is summarized in Figure 7 and Table S10. These data reveal that, as found for the AAs, the relatively tightly bound first layer of water molecules at the aqueous Pd(111) interface (compared with the Au(111) interface) resulted in remarkably different adsorbed conformations of the peptides at the two metal interfaces. At the Au(111) interface, most residues (in both peptides) showed at least some degree of direct contact with the surface. Consequently, both peptides were predicted to lie relatively flat on the Au surface, with the peptide backbone positioned close to the metal interface. In contrast, at the Pd(111) interface both peptides featured relatively few residues in direct contact with the metal surface (predominantly His and Met). The remaining residues, including the hydrophobic residues Leu and Pro, but also Arg, Gly and Thr, exhibited little or no contact with the metal surface. The lack of surface contact for the hydrophobic residues can be explained from the largely repulsive free energy profile determined for Leu, and the weakly-adsorbed profile predicted for Arg (Figure 4). Moreover, the closest position of the peptide backbone with respect to the Pd(111) surface was typically more distant than that predicted for the Au(111) interface, corresponding with the second solvation layer at the Pd interface. This adsorption mode is reminiscent of those reported for peptides adsorbed at the aqueous TiO_2 rutile (110) interface.[96] We propose that if the backbone-surface distance is a general feature of Pd-adsorbed peptides, this limits the type of residues that could (in principle) make direct contact with the Pd(111) interface to those with side-chains of sufficient length to reach the surface. We also compared the residue-surface contact determined from REST-

MD simulations using both the TIP3P and TIP4P-D water models. The overall pattern of residue-surface contact at the Pd(111) interface was broadly consistent across both of these water models.

Our findings are consistent with available experimental evidence. Both the Pd2 and Pd4 peptide sequences feature His and Met, which we predict to both be strong-binding residues at the aqueous Pd(111) interface. Moreover, the importance of the His residues in the adsorption of the peptides is consistent with the findings of previous studies where the mutation of His residues to Ala in Pd4 reduced the binding propensity of the peptide.[97] Overall, while further data are certainly needed, our initial binding data indicate that there may be limited prospects for devising peptide sequences that are truly selective for binding to Pd(111) in preference Au(111). However, in contrast, our findings suggest that a sequence rich in Arg and lacking in Met and His may provide sufficient binding selectivity to confer binding discrimination for Au(111) over Pd(111).

We also analyzed and compared the backbone conformational similarities for both of these sequences and both metal interfaces. At the Au(111) interface, the number of distinct conformations and the distribution of the relative populations of these distinct conformations is similar for Pd2 and Pd4 (data provided in Table S11 and Figure S12 in the Supporting Information). Each sequence adsorbed at Au(111) supported a large number of distinct conformations. Furthermore, even the most populated distinct conformation on Au(111) accounted for less than 20% of the total ensemble population, as has been typically reported for dodecapeptides adsorbed at aqueous noble metal interfaces.[15,20,81] A similar distribution of conformational populations was also predicted for Pd4 adsorbed at the Pd(111) interface. However, Pd2 adsorbed on Pd(111) featured a remarkably different population distribution, with its most populated distinct conformation accounting for $\approx 40\%$ of the total ensemble population. This suggests that Pd2 supports a distinct preferred binding conformation when adsorbed at the aqueous Pd(111) interface. This is an atypical trait compared with most other materials-binding peptides. We also investigated the degree of backbone conforma-

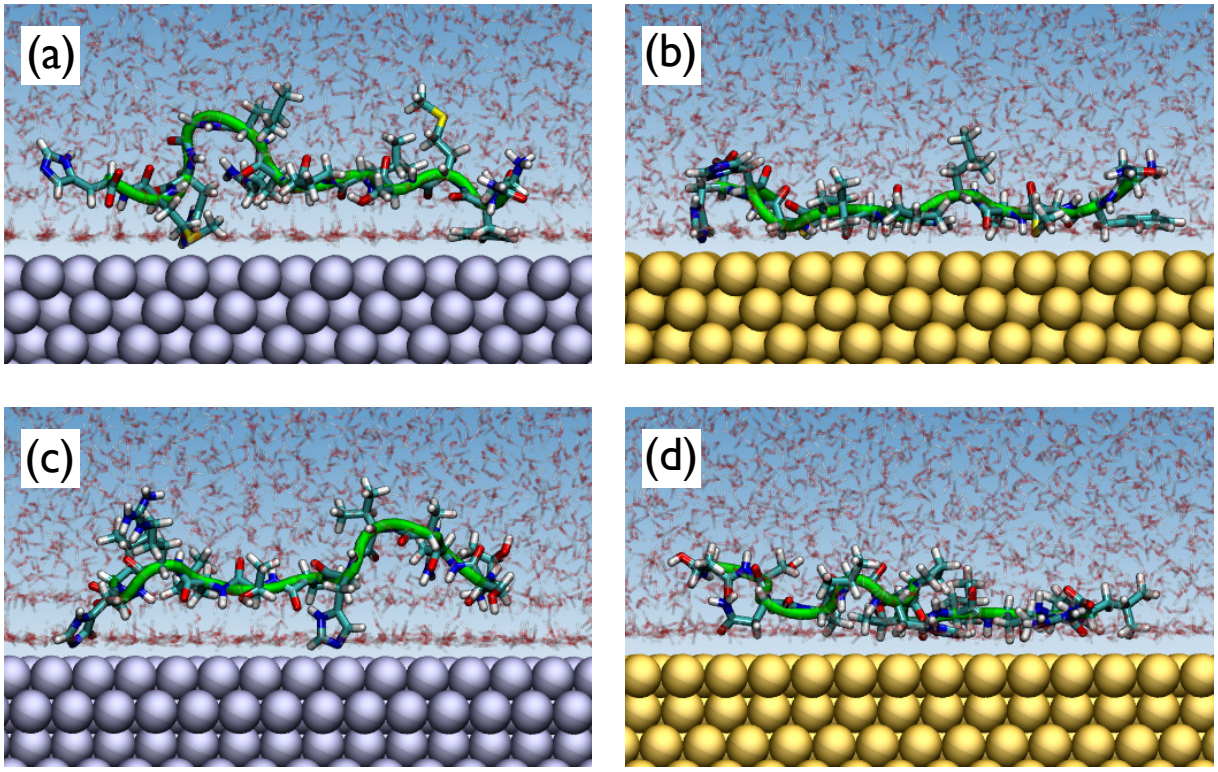

Figure 6: Representative snapshots of the peptide chains adsorbed at the aqueous Pd(111) and Au(111) interfaces, determined from replica exchange with solute tempering molecular dynamics simulations; (a) Pd2 on Pd(111), (b) Pd2 on Au(111), (c) Pd4 on Pd(111) and (d) Pd4 on Au(111).

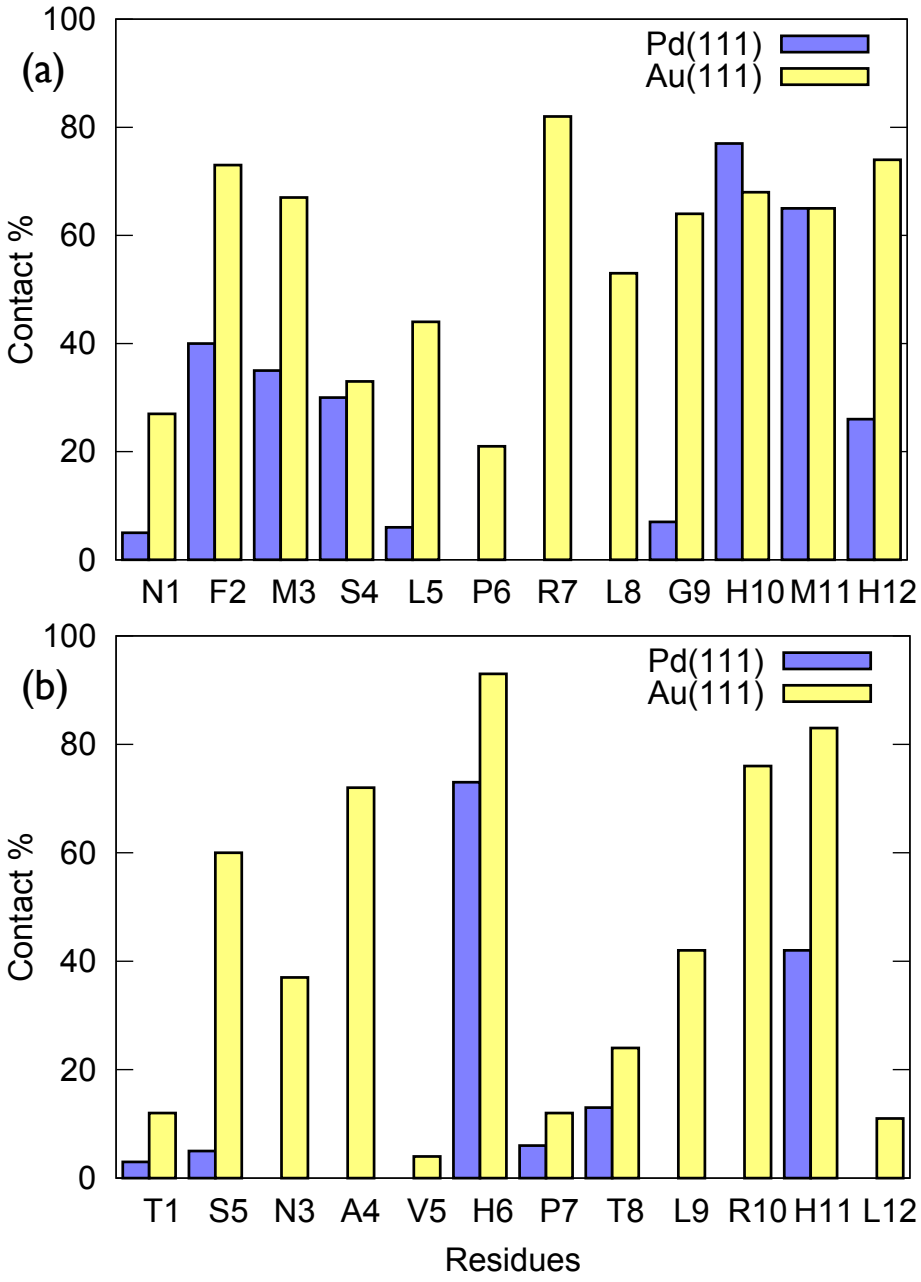

Figure 7: Degree of residue-surface direct contact determined from replica exchange with solute tempering molecular dynamics simulations for (a) Pd2 and (b) Pd4 peptides adsorbed at the aqueous Pd(111) and Au(111) interfaces.

tional similarity between the two peptides when adsorbed at the Pd and Au interfaces. To accomplish this, we determined the number of matched conformations (defined as a RMSD in backbone atom positions < 2 Å, explained in the Supporting Information) representative of the top ten most populated distinct structures, across the Pd/Au interfaces. This comparison allows an estimation of the similarity of the peptide conformational ensembles between the two interfaces. This cross-ensemble analysis (Table S12) revealed very few matches for either peptide across the two metal interfaces, confirming that each peptide featured different conformational ensembles when adsorbed at the Pd and Au surfaces.

The influence of the water model used in our REST-MD simulations was also probed. The use of the TIP4P-D water model was found to somewhat alter the distribution of the conformational ensemble of the peptides. However, the differences observed between the two peptide sequences were consistent across the two water models, with both the total number of distinct conformations and the estimates of the conformational entropic contribution (explained in the Supporting Information) reduced. Notably, the representative conformation of the most populated distinct conformation of Pd2, which accounted for more than 40% of the population, was a match for both water models. This indicates that both water models favored the same, most likely binding conformation. Likewise, the large number of matched distinct conformations of Pd4 across the two water models suggested that, despite the change in water model, the conformational ensemble of the adsorbed peptide had persisted to a significant degree. The main effect of the TIP4P-D water model appeared to be a curtailment of conformations from the long low-population 'tail' of the population distribution.

Overall, our REST MD simulations suggested very different binding characteristics for peptides adsorbed at the Pd(111) and Au(111) aqueous interfaces. We attributed these differences primarily to the presence of the relatively strongly-bound first solvation layer of water molecules at the aqueous Pd(111) interface. Consistent with the experimentally proposed hypothesis regarding Pd4 binding, the results of our simulations indicated the His residues as key binding residues of the Pd2 and Pd4 sequences. Finally, while the use

the TIP4P-D water model, rather than the modified TIP3P water model, does result in some differences in residue-surface contact and conformational population distributions of the adsorbed peptides, the overall binding characteristics of the adsorbed peptides predicted using the two water models was broadly consistent.

Conclusions

In summary, we have devised a new polarizable force-field, PdP-CHARMM, for describing biomolecule interactions at the aqueous Pd(111) interface. To do this, we parametrized our model using density functional theory (DFT) calculations of biomolecule/Pd(111) adsorption using the PBEκ=1-vdW-DF functional. This choice was based on our extensive survey of DFT functionals performed for a wide range of small biomolecules. Molecular dynamics (MD) simulations using this force-field predicted a strongly-bound first interfacial water layer at the aqueous Pd(111) interface. Our force-field was then used to determine the binding free energy for a range of representative amino acids adsorbed at the aqueous Pd(111) interface, revealing a strong preference for His and Met residues, while other residues showed weak binding. We then used replica exchange with solute tempering MD simulations to predict and contrast the conformational ensemble of two known Pd-binding peptide sequences, adsorbed at both the aqueous Pd(111) and Au(111) interfaces. Our simulations indicated remarkable differences in the binding characteristics of these peptides at the two metal interfaces. Specifically, the Pd interface supported a greater degree of relatively three-dimensional conformations mediated by Met and His surface contact, compared with the relatively flat peptide adsorption modes at the Au interface. Our peptide-surface contact data were consistent with experimental findings that suggest the importance of His residues. We suggest that differences in the peptide binding features at the aqueous Pd(111) interface can be largely attributed to the strongly-bound first interfacial solvation layer. The PdP-CHARMM force-field and current findings will contribute to new directions in exploring and

designing peptide sequences with binding selectivity between Au and Pd surfaces.

Acknowledgement

This research was undertaken with the assistance of resources from the National Computational Infrastructure (NCI), which is supported by the Australian Government. The authors thank the Victorian Life Sciences Computation Initiative (VLSCI) for computational resources. We gratefully acknowledge financial support from the Air Force Office for Scientific Research (Grant #FA9550-12-1-0226).

Supporting Information Available

The FF gromacs files are available from the authors upon request. Details of the development of the PdP-CHARMM force-field; methodology of the REST-MD simulations analysis; methodology used for calculation of the free energies of adsorption; super-cells used from the DFT calculations; atoms used as collective variables for AA metadynamics simulations; separation distances, adsorption energies and optimized geometries of adsorbates from the DFT calculations; comparison of in vacuo adsorption energies at Pd(111), Au(111) and Ag(111); adsorption energies and separation distances of adsorbates from in vacuo FF calculations; 2D structuring of water at Pd(111) and Au(111) interfaces; orientational ordering of water at Pd(111) and Au(111) interfaces; density profiles of alternative water models at Pd(111) and Au(111) interfaces; ratio of number of water molecules in first layer to the number of metal atoms; hydrogen bonding profiles of water at Pd(111) and Au(111) interfaces; free energy of adsorption convergence for AA metadynamics simulations; free energy of adsorption profiles of AAs for different water models; snapshots of representative conformations of peptides simulated in TIP4P-D water; residue contact analysis; population distribution of clusters; number of cluster as a function of REST-MD step; cross-cluster structural matches. This material is available free of charge via the Internet at `http://pubs.acs.org/`.

References

(1) Pacardo, D. B.; Sethi, M.; Jones, S. E.; Naik, R. R.; Knecht, M. R. Biomimetic synthesis of Pd nanocatalysts for the Stille coupling reaction. *ACS Nano* **2009**, *3*, 1288–1296.

(2) Yang, X.; Yang, M.; Pang, B.; Vara, M.; Xia, Y. Gold nanomaterials at work in biomedicine. *Chem. Rev.* **2015**, *115*, 10410–10488.

(3) Yan, F.; Liu, L.; Walsh, T. R.; Gong, Y.; El-Khoury, . Z.; Zhang, Y.; Zhu, Z.; Yoreo, J. J. D.; Engelhard, M. H.; Zhang, X. et al. Controlled synthesis of highly-branched plasmonic gold nanoparticles through peptoid engineering. *Nat. Commun.* **2018**, *9*, 2327.

(4) Tamerler, C.; Sarikaya, M. Genetically designed peptide-based molecular materials. *ACS Nano* **2009**, *3*, 1606–1615.

(5) Walsh, T. R.; Knecht, M. R. Biointerface structural effects on the properties and applications of bioinspired peptide-based nanomaterials. *Chem. Rev.* **2017**, *117*, 12641–12704.

(6) Merrill, N. A.; McKee, E. M.; Merino, K. C.; Drummy, L. F.; Lee, S.; Reinhart, B.; Ren, Y.; Frenkel, A. I.; Naik, R. R.; Bedford, N. M. et al. Identifying the atomic-level effects of metal composition on the structure and catalytic activity of peptide-templated materials. *ACS Nano* **2015**, *9*, 11968–11979.

(7) Bedford, N. M.; Showalter, A. R.; Woehl, T. J.; Hughes, Z. E.; Lee, S.; Reinhart, B.; Ertem, S. P.; Coughlin, E. B.; Ren, Y.; Walsh, T. R. et al. Peptide-directed PdAu nanoscale surface segregation: toward controlled bimetallic architecture for catalytic materials. *ACS Nano* **2016**, *10*, 8645–8659.

(8) Gilroy, K. D.; Ruditskiy, A.; Peng, H.-C.; Qin, D.; Xia, Y. Bimetallic nanocrystals: syntheses, properties, and applications. *Chem. Rev.* **2016**, *116*, 10414–10472.

(9) Satyavolu, N. S. R.; Tan, L. H.; Lu, Y. DNA-mediated morphological control of Pd–Au bimetallic nanoparticles. *J. Am. Chem. Soc.* **2016**, *138*, 16542–16548.

(10) Sun, L.; Zhang, Q.; Li, G. G.; Villarreal, E.; Fu, X.; Wang, H. Multifaceted gold–palladium bimetallic nanorods and their geometric, compositional, and catalytic tunabilities. *ACS Nano* **2017**, *11*, 3213–3228.

(11) Hussein, H. A.; Demiroglu, I.; Johnston, R. L. Application of a parallel genetic algorithm to the global optimization of medium-sized Au-Pd sub-nanometre clusters. *Euro. Phys. J. B* **2018**, *91*, 34.

(12) Heinz, H.; Farmer, B. L.; Pandey, R. B.; Slocik, J. M.; Patnaik, S. S.; Pachter, R.; Naik, R. R. Nature of molecular interactions of peptides with gold, palladium, and Pd-Au bimetal surfaces in aqueous solution. *J. Am. Chem. Soc.* **2009**, *131*, 9704–9714.

(13) Pandey, R. B.; Heinz, H.; Feng, J.; Farmer, B. L.; Slocik, J. M.; Drummy, L. F.; Naik, R. R. Adsorption of peptides (A3, Flg, Pd2, Pd4) on gold and palladium surfaces by a coarse-grained Monte Carlo simulation. *Phys. Chem. Chem. Phys.* **2009**, *11*, 1989–2001.

(14) Feng, J.; Slocik, J. M.; Sarikaya, M.; Naik, R. R.; Farmer, B. L.; Heinz, H. Influence of the shape of nanostructured metal surfaces on adsorption of single peptide molecules in aqueous solution. *Small* **2012**, *8*, 1049–1059.

(15) Tang, Z.; Palafox-Hernandez, J. P.; Law, W.-C.; Hughes, Z. E.; Swihart, M. T.; Prasad, P. N.; Knecht, M. R.; Walsh, T. R. Biomolecular recognition principles for bionanocombinatorics: an integrated approach to elucidate enthalpic and entropic factors. *ACS Nano* **2013**, *7*, 9632–9646.

(16) Wright, L. B.; Rodger, P. M.; Corni, S.; Walsh, T. R. GolP-CHARMM: first-principles based force fields for the interaction of proteins with Au(111) and Au(100). *J. Chem. Theory Comput.* **2013**, *9*, 1616–1630.

(17) Wright, L. B.; Rodger, P. M.; Walsh, T. R.; Corni, S. First-principles-based force field for the interaction of proteins with Au(100)(5 × 1): an extension of GolP-CHARMM. *J. Phys. Chem. C* **2013**, *117*, 24292–24306.

(18) Hughes, Z. E.; Wright, L. B.; Walsh, T. R. Biomolecular adsorption at aqueous silver interfaces: first-principles calculations, polarizable force-field simulations, and comparisons with gold. *Langmuir* **2013**, *29*, 13217–13229.

(19) Hughes, Z. E.; Walsh, T. R. Structure of the electrical double layer at aqueous gold and silver interfaces for saline solutions. *J. Colloid Interface Sci.* **2014**, *436*, 99–110.

(20) Palafox-Hernandez, J. P.; Tang, Z.; Hughes, Z. E.; Li, Y.; Swihart, M. T.; Prasad, P. N.; Walsh, T. R.; Knecht, M. R. Comparative study of materials-binding peptide interactions with gold and silver surfaces and nanostructures: a thermodynamic basis for biological selectivity of inorganic materials. *Chem. Mater.* **2014**, *26*, 4960–4969.

(21) Bedford, N. M.; Ramezani-Dakhel, H.; Slocik, J. M.; Briggs, B. D.; Ren, Y.; Frenkel, A. I.; Petkov, V.; Heinz, H.; Naik, R. R.; Knecht, M. R. Elucidation of peptide-directed palladium surface structure for biologically tunable nanocatalysts. *ACS Nano* **2015**, *9*, 5082–5092.

(22) Nash, J. A.; Singh, A.; Li, N. K.; Yingling, Y. G. Characterization of nucleic acid compaction with histone-mimic nanoparticles through all-atom molecular dynamics. *ACS Nano* **2015**, *9*, 12374–12382.

(23) Wright, L. B.; Palafox-Hernandez, J. P.; Rodger, P. M.; Corni, S.; Walsh, T. R. Facet selectivity in gold binding peptides: exploiting interfacial water structure. *Chem. Sci.* **2015**, *6*, 5204–5214.

(24) Ozboyaci, M.; Kokh, D. B.; Corni, S.; Wade, R. C. Modeling and simulation of protein-surface interactions: achievements and challenges. *Q. Rev. Biophys.* **2016**, *49*, e4.

(25) Monti, S.; Carravetta, V.; Ågren, H. Simulation of gold functionalization with cysteine by reactive molecular dynamics. *J. Phys. Chem. Lett.* **2016**, *7*, 272–276.

(26) Bellucci, L.; Bussi, G.; Di Felice, R.; Corni, S. Fibrillation-prone conformations of the amyloid-β-42 peptide at the gold/water interface. *Nanoscale* **2017**, *9*, 2279–2290.

(27) Hughes, Z. E.; Kochandra, R.; Walsh, T. R. Facet-specific adsorption of tripeptides at aqueous Au interfaces: open questions in reconciling experiment and simulation. *Langmuir* **2017**, *33*, 3742–3754.

(28) Gupta, M.; Khan, T. S.; Agarwal, M.; Haider, M. A. Understanding the nature of amino acid interactions with Pd(111) or Pd–Au bimetallic catalysts in the aqueous phase. *Langmuir* **2018**, *34*, 1300–1310.

(29) Iori, F.; Di Felice, R.; Molinari, E.; Corni, S. GolP: An atomistic force-field to describe the interaction of proteins with Au(111) surfaces in water. *J. Comput. Chem.* **2009**, *30*, 1465–1476.

(30) Iori, F.; Corni, S. Including image charge effects in the molecular dynamics simulations of molecules on metal surfaces. *J. Comput. Chem.* **2008**, *29*, 1656–1666.

(31) Skelton, A. A.; Liang, T.; Walsh, T. R. Interplay of sequence, conformation, and binding at the peptide-titania interface as mediated by water. *ACS Appl. Mater. Interfaces* **2009**, *1*, 1482–1491.

(32) Schneider, J.; Colombi Ciacchi, L. Specific material recognition by small peptides mediated by the interfacial solvent structure. *J. Am. Chem. Soc.* **2012**, *134*, 2407–2413.

(33) Limmer, D. T.; Willard, A. P.; Madden, P.; Chandler, D. Hydration of metal surfaces can be dynamically heterogeneous and hydrophobic. *Proc. Natl. Acad. Sci. U.S.A* **2013**, *110*, 4200–4205.

(34) Michaelides, A.; Ranea, V.; de Andres, P.; King, D. General model for water monomer adsorption on close-packed transition and noble metal surfaces. *Phys. Rev. Lett.* **2003**, *90*, 216102.

(35) Michaelides, A.; Alavi, A.; King, D. Insight into H_2O-ice adsorption and dissociation on metal surfaces from first-principles simulations. *Phys. Rev. B* **2004**, *69*, 113404.

(36) Carrasco, J.; Michaelides, A.; Scheffler, M. Insight from first principles into the nature of the bonding between water molecules and 4d metal surfaces. *J. Chem. Phys.* **2009**, *130*, 184707.

(37) Tereshchuk, P.; Da Silva, J. L. F. Ethanol and water adsorption on close-packed 3d, 4d, and 5d transition-metal surfaces: a density functional theory investigation with van der Waals correction. *J. Phys. Chem. C* **2012**, *116*, 24695–24705.

(38) Carrasco, J.; Klimeš, J.; Michaelides, A. The role of van der Waals forces in water adsorption on metals. *J. Chem. Phys.* **2013**, *138*, 024708.

(39) Schnur, S.; Groß, A. Properties of metal–water interfaces studied from first principles. *New J. Phys.* **2009**, *11*, 125003.

(40) Pedroza, L. S.; Poissier, A.; Fernández-Serra, M. V. Local order of liquid water at metallic electrode surfaces. *J. Chem. Phys.* **2015**, *142*, 034706.

(41) Bellarosa, L.; García-Muelas, R.; Revilla-López, G.; López, N. Diversity at the water–metal interface: metal, water thickness, and confinement effects. *ACS Cent. Sci.* **2016**, *2*, 109–116.

(42) Jorgensen, W. L.; Chandrasekhar, J.; Madura, J. D.; Impey, R. W.; Klein, M. L. Comparison of simple potential functions for simulating liquid water. *J. Chem. Phys.* **1983**, *79*, 926–935.

(43) Neria, E.; Fischer, S.; Karplus, M. Simulation of activation free energies in molecular systems. *J. Chem. Phys.* **1996**, *105*, 1902–1921.

(44) Nerenberg, P. S.; Head-Gordon, T. Optimizing protein–solvent force fields to reproduce intrinsic conformational preferences of model peptides. *J. Chem. Theory Comput.* **2011**, *7*, 1220–1230.

(45) Nerenberg, P. S.; Jo, B.; So, C.; Tripathy, A.; Head-Gordon, T. Optimizing solute–water van der Waals interactions to reproduce solvation free energies. *J. Phys. Chem. B* **2012**, *116*, 4524–4534.

(46) Best, R. B.; Zheng, W.; Mittal, J. Correction to Balanced Protein–Water interactions improve properties of disordered proteins and non-specific protein association. *J. Chem. Theory Comput.* **2015**, *11*, 1978–1978.

(47) Piana, S.; Donchev, A. G.; Robustelli, P.; Shaw, D. E. Water dispersion interactions strongly influence simulated structural properties of disordered protein states. *J. Phys. Chem. B* **2015**, *119*, 5113–5123.

(48) Huang, J.; Rauscher, S.; Nawrocki, G.; Ran, T.; Feig, M.; de Groot, B. L.; Grubmüller, H.; MacKerell, A. D. CHARMM36m: an improved force field for folded and intrinsically disordered proteins. *Nat. Methods* **2016**, *14*, 71–73.

(49) Henriques, J.; Skepö, M. Molecular dynamics simulations of intrinsically disordered proteins: on the accuracy of the TIP4P-D water model and the representativeness of protein disorder models. *J. Chem. Theory Comput.* **2016**, *12*, 3407–3415.

(50) Desmond, J. L.; Rodger, P. M.; Walsh, T. R. Testing the inter-operability of the CHARMM and SPC/Fw force fields for conformational sampling. *Mol. Simul.* **2013**, *40*, 912–921.

(51) Dion, M.; Rydberg, H.; Schröder, E.; Langreth, D. C.; Lundqvist, B. I. van der Waals density functional for general geometries. *Phys. Rev. Lett.* **2004**, *92*, 246401.

(52) Thonhauser, T.; Zuluaga, S.; Arter, C. A.; Berland, K.; Schröder, E.; Hyldgaard, P. Spin signature of nonlocal correlation binding in metal-organic frameworks. *Phys. Rev. Lett.* **2015**, *115*, 136402.

(53) Liu, W.; Carrasco, J.; Santra, B.; Michaelides, A.; Scheffler, M.; Tkatchenko, A. Benzene adsorbed on metals: concerted effect of covalency and van der Waals bonding. *Phys. Rev. B* **2012**, *86*, 245405.

(54) Rosa, M.; Corni, S.; Di Felice, R. Interaction of nucleic acid bases with the Au(111) surface. *J. Chem. Theory Comput.* **2013**, *9*, 4552–4561.

(55) Carrasco, J.; Liu, W.; Michaelides, A.; Tkatchenko, A. Insight into the description of van der Waals forces for benzene adsorption on transition metal (111) surfaces. *J. Chem. Phys.* **2014**, *140*, 084704.

(56) Hughes, Z. E.; Walsh, T. R. Non-covalent adsorption of amino acid analogues on noble-metal nanoparticles: influence of edges and vertices. *Phys. Chem. Chem. Phys.* **2016**, *18*, 17525–17533.

(57) Hughes, Z. E.; Baev, A.; Prasad, P. N.; Walsh, T. R. Halo-substituted azobenzenes adsorbed at Ag(111) and Au(111) interfaces: Structures and optical properties. *Phys. Rev. B* **2017**, *95*, 205425.

(58) Giannozzi, P.; Baroni, S.; Bonini, N.; Calandra, M.; Car, R.; Cavazzoni, C.; Ceresoli, D.; Chiarotti, G. L.; Cococcioni, M.; Dabo, I.; *et al.*, QUANTUM ESPRESSO: a modular and open-source software project for quantum simulations of materials. *J. Phys. Condens. Matter* **2009**, *21*, 395502.

(59) Klimeš, J.; Bowler, D. R.; Michaelides, A. Chemical accuracy for the van der Waals density functional. *J. Phys.: Condens. Matter* **2010**, *22*, 022201.

(60) Klimeš, J.; Bowler, D. R.; Michaelides, A. Van der Waals density functionals applied to solids. *Phys. Rev. B* **2011**, *83*, 195131.

(61) Cooper, V. R. Van der Waals density functional: An appropriate exchange functional. *Phys. Rev. B* **2010**, *81*, 161104.

(62) Berland, K.; Hyldgaard, P. Exchange functional that tests the robustness of the plasmon description of the van der Waals density functional. *Phys. Rev. B* **2014**, *89*, 035412.

(63) Lee, K.; Murray, É. D.; Kong, L.; Lundqvist, B. I.; Langreth, D. C. Higher-accuracy van der Waals density functional. *Phys. Rev. B* **2010**, *82*, 081101.

(64) Hamada, I. van der Waals density functional made accurate. *Phys. Rev. B* **2014**, *89*, 121103(R).

(65) Vydrov, O. A.; Van Voorhis, T. Dispersion interactions from a local polarizability model. *Phys. Rev., A* **2010**, *81*, 062708.

(66) Sabatini, R.; Gorni, T.; De Gironcoli, S. Nonlocal van der Waals density functional made simple and efficient. *Phys. Rev. B* **2013**, *87*, 041108(R).

(67) MacKerell, A. D., Jr; Bashford, D.; Bellott, M.; Dunbrack, R. L., Jr; Evanseck, J. D.; Field, M. J.; Fischer, S.; Gao, J.; Guo, H.; Ha, S. All-atom empirical potential for molecular modeling and dynamics studies of proteins. *J. Phys. Chem. B* **1998**, *102*, 3586–3616.

(68) Piana, S.; Lindorff-Larsen, K.; Shaw, D. E. How robust are protein folding simulations with respect to force field parameterization? *Biophys. J.* **2011**, *100*, L47–L49.

(69) Abraham, M. J.; Murtola, T.; Schulz, R.; Páll, S.; Smith, J. C.; Hess, B.; Lindahl, E. GROMACS: High performance molecular simulations through multi-level parallelism from laptops to supercomputers. *SoftwareX* **2015**, *1-2*, 19–25.

(70) Tribello, G. A.; Bonomi, M.; Branduardi, D. PLUMED 2: New feathers for an old bird. *Comput. Phys. Comm.* **2014**, *185*, 606–613.

(71) Nosé, S. A unified formulation of the constant temperature molecular dynamics methods. *J. Chem. Phys.* **1984**, *81*, 511–519.

(72) Hoover, W. Canonical dynamics: Equilibrium phase-space distributions. *Phys. Rev. A* **1985**, *31*, 1695–1697.

(73) Darden, T.; York, D.; Pedersen, L. Particle mesh ewald - an N.Log(N) method for ewald sums in large systems. *J. Chem. Phys.* **1993**, *98*, 10089–10092.

(74) Wu, Y.; Tepper, H. L.; Voth, G. A. Flexible simple point-charge water model with improved liquid-state properties. *J. Chem. Phys.* **2006**, *124*, 024503.

(75) Laio, A.; Parrinello, M. Escaping free-energy minima. *Proc. Natl. Acad. Sci. USA* **2002**, *99*, 12562–12566.

(76) Barducci, A.; Bussi, G.; Parrinello, M. Well-tempered metadynamics: a smoothly converging and tunable free-energy method. *Phys. Rev. Lett.* **2008**, *100*, 020603.

(77) Raiteri, P.; Laio, A.; Gervasio, F. L.; Micheletti, C.; Parrinello, M. Efficient reconstruction of complex free energy landscapes by multiple walkers metadynamics. *J. Phys. Chem. B* **2006**, *110*, 3533–3539.

(78) O'Brien, C. P.; Stuart, S. J.; Bruce, D. A.; Latour, R. A. Modeling of peptide adsorption interactions with a poly(lactic acid) surface. *Langmuir* **2008**, *24*, 14115–14124.

(79) Terakawa, T.; Kameda, T.; Takada, S. On easy implementation of a variant of the replica exchange with solute tempering in GROMACS. *J. Comput. Chem.* **2010**, *32*, 1228–1234.

(80) Wright, L. B.; Walsh, T. R. Efficient conformational sampling of peptides adsorbed onto inorganic surfaces: insights from a quartz binding peptide. *Phys. Chem. Chem. Phys.* **2013**, *15*, 4715–4726.

(81) Hughes, Z. E.; Nguyen, M. A.; Li, Y.; Swihart, M. T.; Walsh, T. R.; Knecht, M. R. Elucidating the influence of materials-binding peptide sequence on Au surface interactions and colloidal stability of Au nanoparticles. *Nanoscale* **2017**, *9*, 421–432.

(82) Gautier, S.; Steinmann, S. N.; Michel, C.; Fleurat-Lessard, P.; Sautet, P. Molecular adsorption at Pt(111). How accurate are DFT functionals? *Phys. Chem. Chem. Phys.* **2015**, *17*, 28921–28930.

(83) Antony, A.; Hakanoglu, C.; Asthagiri, A.; Weaver, J. F. Dispersion-corrected density functional theory calculations of the molecular binding of n-alkanes on Pd(111) and PdO(101). *J. Chem. Phys.* **2012**, *136*, 054702.

(84) García-Muelas, R.; López, N. Collective descriptors for the adsorption of sugar alcohols on Pt and Pd(111). *J. Phys. Chem. C* **2014**, *118*, 17531–17537.

(85) Davis, J. L.; Barteau, M. A. Decarbonylation and decomposition pathways of alcohols on Pd (111). *Surface Science* **1987**, *187*, 387–406.

(86) Tysoe, W. T.; Ormerod, R. M.; Lambert, R. M.; Zgrablich, G.; Ramirez-Cuesta, A. Overlayer structure and kinetic behavior of benzene on palladium (111). *J. Phys. Chem.* **1993**, *97*, 3365–3370.

(87) Liu, W.; Tkatchenko, A.; Scheffler, M. Modeling adsorption and reactions of organic molecules at metal surfaces. *Acc. Chem. Res.* **2014**, *47*, 3369–3377.

(88) Ghiringhelli, L. M.; Delle Site, L. Phenylalanine near inorganic surfaces: conformational statistics vs specific chemistry. *J. Amer. Chem. Soc.* **2008**, *130*, 2634–2638.

(89) Hughes, Z. E.; Tomásio, S. M.; Walsh, T. R. Efficient simulations of the aqueous bio-interface of graphitic nanostructures with a polarisable model. *Nanoscale* **2014**, *6*, 5438–5448.

(90) Nadler, R.; Sanz, J. F. Effect of dispersion correction on the Au(111)-H_2O interface: a first-principles study. *J. Chem. Phys.* **2012**, *137*, 114709.

(91) Cicero, G.; Calzolari, A.; Corni, S.; Catellani, A. Anomalous wetting layer at the Au (111) surface. *J. Phys. Chem. Lett.* **2011**, *2*, 2582–2586.

(92) Björneholm, O.; Hansen, M. H.; Hodgson, A.; Liu, L.-M.; Limmer, D. T.; Michaelides, A.; Pedevilla, P.; Rossmeisl, J.; Shen, H.; Tocci, G. et al. Water at interfaces. *Chem. Rev.* **2016**, *116*, 7698–7726.

(93) Gillan, M. J.; Alfè, D.; Michaelides, A. Perspective: how good is DFT for water? *J. Chem. Phys.* **2016**, *144*, 130901.

(94) Schravendijk, P.; van der Vegt, N.; Delle Site, L.; Kremer, K. Dual-scale modeling of benzene adsorption onto Ni(111) and Au(111) surfaces in explicit water. *ChemPhysChem* **2005**, *6*, 1866–1871.

(95) Schravendijk, P.; Ghiringhelli, L. M.; Delle Site, L.; van der Vegt, N. Interaction of hydrated amino acids with metal surfaces: a multiscale modeling description. *J. Phys. Chem. C* **2007**, *111*, 2631–2642.

(96) Sultan, A. M.; Westcott, Z. C.; Hughes, Z. E.; Palafox-Hernandez, J. P.; Giesa, T.; Puddu, V.; Buehler, M. J.; Perry, C. C.; Walsh, T. R. Aqueous peptide–TiO_2 interfaces: isoenergetic binding via either entropically or enthalpically driven mechanisms. *ACS Appl. Mater. Interfaces* **2016**, *8*, 18620–18630.

(97) Coppage, R.; Slocik, J. M.; Ramezani-Dakhel, H.; Bedford, N. M.; Heinz, H.; Naik, R. R.; Knecht, M. R. Exploiting localized surface binding effects to enhance the catalytic reactivity of peptide-capped nanoparticles. *J. Am. Chem. Soc.* **2013**, *135*, 11048–11054.

Graphical TOC Entry